同行专家业内评价意见书编号：20250858280

附件1

浙江工程师学院（浙江大学工程师学院）
同行专家业内评价意见书

姓名：沈曦

学号：22260143

申报工程师职称专业类别（领域）：能源动力

浙江工程师学院（浙江大学工程师学院）制

2025年05月30日

填表说明

一、本报告中相关的技术或数据如涉及知识产权保护、军工项目保密等内容，请作脱密处理。

二、请用宋体小四字号撰写本报告，可另行附页或增加页数，A4纸双面打印。

三、表中所涉及的签名都必须用蓝、黑色墨水笔，亲笔签名或签字章，不可以打印代替。

四、同行专家业内评价意见书编号由工程师学院填写，编号规则为：年份4位＋申报工程师职称专业类别(领域)4位+流水号3位，共11位。

一、个人申报

（一）基本情况【围绕《浙江工程师学院（浙江大学工程师学院）工程类专业学位研究生工程师职称评审参考指标》，结合该专业类别(领域)工程师职称评审相关标准，举例说明】

1.对本专业基础理论知识和专业技术知识掌握情况(不少于200字)

在研究304奥氏体不锈钢氢致裂纹行为的过程中，在导师的指导下，我逐步加深了对材料力学性能分析、氢脆机理和应力-应变关系等相关理论知识的理解，并尝试将所学知识应用于具体的试验研究中。在此过程中，我学习并掌握了声发射无损检测技术的基本原理与应用流程，同时结合课题需求，尝试使用短时傅里叶变换（STFT）、DBSCAN聚类算法与卷积神经网络（CNN）等方法对声信号进行处理与分析。通过这些工作，我逐步提升了在数学建模、信号特征提取和智能识别方面的能力，也加深了对自然科学理论在工程问题中实际作用的认识。

论文工作紧密结合国家重点研发计划“氢能技术”专项的实际需求，聚焦于氢储运系统中材料损伤早期预警技术的发展方向。在开展研究的过程中，我查阅了大量国内外相关文献，了解了当前氢能装备在极端工况下常见的失效模式及声发射在裂纹监测中的应用现状，从而对这一领域的技术趋势、常用标准和工程实践有了初步认识，也为后续研究打下了一定的理论与技术基础。

在与课题组及企业团队的联合研究过程中，我参与了实验方案的制定与实施，包括试样准备、传感器布设、低温环境搭建、数据采集和模型训练等环节。在此过程中，我积累了一些应对实验中突发情况的经验，例如应对温控异常、信号干扰、设备安装偏差等问题。虽然仍有不少地方需要改进和提升，但通过这些实践，我逐步增强了将理论知识应用于工程实际的能力，也提高了自己在任务执行过程中的稳定性和抗压能力。

此外，在材料试验和现场测试的具体操作中，我对传感器布设、耦合材料选择和信号采集质量控制等方面进行了反复尝试和调整，逐渐建立起对实验误差来源的基本判断能力。在老师和企业工程师的帮助下，我也逐步理解了设备调试中的注意事项，并在实践中锻炼了在复杂环境下应对问题的能力。通过亲身参与这些环节，我对“现场经验”的重要性有了更深的体会，并逐步建立起较为朴素但实用的工程直觉。

在数据分析和建模方面，我学习使用MATLAB进行力学数据处理，使用Python完成信号的频域转换与神经网络建模。这些工作虽然还有待进一步优化和深入，但在一定程度上帮助我提升了将理论工具应用于实际数据分析和问题求解的能力，也让我认识到多学科交叉背景在工程问题中的实际意义。

2.工程实践的经历(不少于200字)

本人在硕士研究期间，参与了国家重点研发计划“氢能技术”重点专项课题《纯氢与天然气掺氢长输管道输送及应用关键技术》（项目编号：2022YFB4003400）中的子课题研究，主要围绕氢储运过程中压力容器结构材料的损伤监测方法开展相关工作。在导师和课题组的指导下，我完成了“基于声发射技术与深度学习的氢致裂纹识别方法研究”的研究任务，积累了一定的工程实践经验。

在项目实施过程中，我参与了304奥氏体不锈钢在不同温度和充氢条件下的力学性能测试、裂纹形貌观察和声发射数据采集等实验工作，并尝试进行信号特征提取及初步的模型构建。

实验中使用了Instron液压拉伸设备、工业CT系统、HIDEN
TPD氢含量分析平台等常用设备，同时也完成了低温拉伸环境下的设备安装与调试、试样处理、数据采集和系统日常维护等环节，较好地锻炼了我对实验全过程的把控能力。

在数据分析与模型探索方面，我尝试基于实验需求，搭建了一个结合短时傅里叶变换（STFT）、DBSCAN聚类算法与卷积神经网络（CNN）模型的识别流程，初步实现了对声发射信号的分类识别。这一尝试在一定程度上提高了识别准确率，并对复杂背景下的噪声过滤提出了可行性思路，为后续开展在线监测系统研究提供了一些基础参考。

此外，在项目执行过程中，我积极参与了与企业合作团队的技术交流，配合撰写了相关技术测试方案、实验记录和阶段性工作总结。通过这些实践，我不仅提升了自身解决实际问题的能力，也更加深刻地认识到科研成果转化为工程应用所面临的挑战和所需的严谨性。

3.在实际工作中综合运用所学知识解决复杂工程问题的案例（不少于1000字）

在参与国家重点研发计划“氢能技术”专项课题《纯氢与天然气掺氢长输管道输送及应用关键技术》（项目编号：2022YFB4003400）的过程中，我有幸参与到“氢致裂纹监测方法研究”相关内容的工作中。在导师指导下，我结合自己在材料力学、信号处理和深度学习等方面的学习积累，尝试围绕氢环境下不锈钢结构损伤的识别问题，开展了一些探索性实践。

本课题的核心难点在于如何实现对裂纹萌生与扩展过程的实时监测。传统的材料断口分析和CT观察虽能揭示裂纹形貌，但多为后验手段，难以满足在线诊断的需要。在导师的建议下，我尝试将声发射技术与深度学习方法结合，探索构建一种较为智能的裂纹识别流程。

在具体工作中，我从实验设计出发，参与了304奥氏体不锈钢在不同温度（室温、218.15K和83.15K）和充氢条件下的慢应变速率拉伸实验。通过对比分析应力-
应变曲线变化，我学习并理解了温度和氢含量对材料弹性模量、屈服强度和断裂韧性的影响，为后续声发射信号特征的分析提供了物理基础。

在数据采集阶段，我协助完成了声发射传感器的布设与系统调试，使用了PCI-
2声发射系统进行多通道信号记录。由于低温环境对耦合剂性能、信号质量有较大影响，我查阅资料、请教经验，尝试筛选合适的材料和安装方式，以尽量保证数据的有效性和一致性。

在数据处理部分，我学习使用MATLAB和Python进行信号预处理与时频分析，并在老师指导下采用短时傅里叶变换（STFT）将信号转换为图像形式，从中提取频谱质心、频带能量比等特征参数。我尝试使用DBSCAN无监督聚类方法进行初步分类，再基于卷积神经网络（CNN）模型进行训练识别。通过不断调整结构和参数，最终模型识别准确率达到95%以上。

尽管仍是初步研究阶段，但实验结果表明，不同裂纹阶段的声发射信号确实存在明显的时频特征差异，深度学习方法也展现出一定的识别潜力。后续我协助整理了实验方案、撰写了部分阶段性汇报材料，也参与了与企业合作团队的几次技术交流，对该技术未来向实际工程推广的条件与挑战有了更清晰的认识。

这次工程实践经历让我深刻体会到理论与实际之间的差距，也让我认识到工程问题往往涉及多个学科的综合运用。从声发射的物理原理，到算法实现的逻辑推理，再到实验设备的操作

细节，每一个环节都需要持续的学习和调整。虽然自己仍处在学习阶段，但通过本次项目的参与，我更加坚定了将专业知识应用于实际工程问题解决的信心，也为后续继续深耕相关方向打下了一定基础。

（二）取得的业绩（代表作）【限填3项，须提交证明原件（包括发表的论文、出版的著作、专利证书、获奖证书、科技项目立项文件或合同、企业证明等）供核实，并提供复印件一份】

1.
公开成果代表作【论文发表、专利成果、软件著作权、标准规范与行业工法制定、著作编写、科技成果获奖、学位论文等】

成果名称	成果类别 [含论文、授权专利（含发明专利申请）、软件著作权、标准、工法、著作、获奖、学位论文等]	发表时间/授权或申请时间等	刊物名称/专利授权或申请号等	本人排名/总人数	备注
INVESTIGATION OF HYDROGEN EMBRITTLEMENT IN 304 AUSTENITIC STAINLESS STEEL THROUGH ACOUSTIC EMISSION MONITORING AND DEEP LEARNING	会议论文	2024年07月28日	Proceedings of the ASME 2024 Pressure Vessels & Piping Conference		

2.其他代表作【主持或参与的课题研究项目、科技成果应用转化推广、企业技术难题解决方案、自主研发设计的产品或样机、技术报告、设计图纸、软课题研究报告、可行性研究报告、规划设计方案、施工或调试报告、工程实验、技术培训教材、推动行业发展中发挥的作用及取得的经济社会效益等】

在读硕期间，我参与了国家重点研发计划“氢能技术”重点专项课题《纯氢与天然气掺氢长输管道输送及应用关键技术》（项目编号：2022YFB4003400）中的子课题工作，研究方向聚焦于氢储运装备结构材料的损伤监测方法。在课题组指导下，我围绕“氢致裂纹的声发射识别方法”开展研究工作，并承担了数据采集、特征分析、模型构建等具体任务，形成了一套基于“STFT特征提取 + DBSCAN聚类 + CNN分类模型”的识别技术流程，为后续成果转化和推广应用奠定了基础。

在该项目的推进过程中，我参与撰写了多份实验设计文档和技术报告，并配合企业技术团队开展低温试验条件下的设备布设、传感器安装及信号校准工作。

实验表明，构建的模型在裂纹信号分类准确率方面具有一定优势，并对部分含噪声信号也展现出良好的识别能力。

（三）在校期间课程、专业实践训练及学位论文相关情况	
课程成绩情况	按课程学分核算的平均成绩： 87 分
专业实践训练时间及考核情况(具有三年及以上工作经历的不作要求)	累计时间： 1 年（要求1年及以上） 考核成绩： 82 分
本人承诺	
个人声明：本人上述所填资料均为真实有效，如有虚假，愿承担一切责任，特此声明！ **申报人签名：** 沈曦	

22260143

二、日常表现考核评价及申报材料审核公示结果

日常表现考核评价	非定向生由德育导师考核评价、定向生由所在工作单位考核评价： ☐优秀　☑良好　☐合格　☐不合格 德育导师/定向生所在工作单位分管领导签字（公章）：周水笛　2025年5月30日
申报材料审核公示	根据评审条件，工程师学院已对申报人员进行材料审核（学位课程成绩、专业实践训练时间及考核、学位论文、代表作等情况），并将符合要求的申报材料在学院网站公示不少于5个工作日，具体公示结果如下： ☐通过　☐不通过（具体原因：　） 工程师学院教学管理办公室审核签字（公章）：　年　月　日

浙 江 大 学 研 究 生 院

攻读硕士学位研究生成绩表

学号：22260143	姓名：沈曦	性别：女	学院：工程师学院	专业：能源动力	学制：2.5年
毕业时最低应获：24.0学分		已获得：27.0学分		入学年月：2022-09	毕业年月：
学位证书号：			毕业证书号：		授予学位：

学习时间	课程名称	备注	学分	成绩	课程性质	学习时间	课程名称	备注	学分	成绩	课程性质
2022-2023学年秋季学期	新时代中国特色社会主义理论与实践		2.0	89	公共学位课	2022-2023学年冬季学期	产业技术发展前沿		1.5	86	专业学位课
2022-2023学年秋季学期	工程技术创新前沿		1.5	90	专业学位课	2022-2023学年春季学期	电气装备健康管理		2.0	81	专业选修课
2022-2023学年秋季学期	新能源发电与变流技术		2.0	94	专业学位课	2022-2023学年春季学期	自然辩证法概论		1.0	84	公共学位课
2022-2023学年冬季学期	低碳能源系统理论与设计		2.0	89	专业选修课	2022-2023学年夏季学期	研究生英语基础技能		1.0	82	公共学位课
2022-2023学年秋冬学期	工程伦理		2.0	89	公共学位课	2022-2023学年春夏学期	高阶工程认知实践		3.0	80	专业选修课
2022-2023学年冬季学期	综合能源系统集成优化		2.0	92	专业学位课	2022-2023学年夏季学期	研究生英语		2.0	80	公共学位课
2022-2023学年秋冬学期	研究生论文写作指导		1.0	88	专业学位课		硕士生读书报告		2.0	通过	
2022-2023学年冬季学期	工程中的有限元方法		2.0	96	专业选修课						

说明：1.研究生课程按三种方法计分：百分制，两级制（通过、不通过），五级制（优、良、中、及格、不及格）。

2.备注中“*”表示重修课程。

学院成绩校核章：

成绩校核人：张梦依

打印日期：2025-06-03

浙江大学研究生院 (60) 成绩校核章

Proceedings of the ASME 2024
Pressure Vessels & Piping Conference
PVP2024
July 29-August 2, 2024, Bellevue, Washington

PVP2024-122737

INVESTIGATION OF HYDROGEN EMBRITTLEMENT IN 304 AUSTENITIC STAINLESS STEEL THROUGH ACOUSTIC EMISSION MONITORING AND DEEP LEARNING

Zhengli Hua
Institute of Process Equipment, Zhejiang University, Hangzhou, P. R. China

Xi Shen
Institute of Process Equipment, Zhejiang University, Hangzhou, P. R. China

Chen Sun
State Power Investment Corporation, Research Institute Co., Ltd., Beijing 102209, China

Meng Xu
State Power Investment Corporation, Research Institute Co., Ltd., Beijing 102209, China

Xing Li
State Power Investment Corporation, Research Institute Co., Ltd., Beijing 102209, China

Wentao Yu
State Power Investment Corporation, Research Institute Co., Ltd., Beijing 102209, China

ABSTRACT

In this academic investigation, we employed Acoustic Emission (AE) monitoring and a Convolutional Neural Network (CNN) to scrutinize hydrogen-induced crack behavior in hydrogen-precharged 304 austenitic stainless steel during tensile stress. This study's pivotal findings reveal that AE monitoring adeptly captures sound wave signal alterations induced by material stress, especially during the critical phase of crack initiation, from the late stage of strengthening to the necking stage. Additionally, industrial-grade Computed Tomography (CT) scans corroborated the presence of a singular principal crack during these phases, aligning with the crack type identified through unsupervised clustering analysis of Short-Time Fourier Transform（STFT）-processed AE signals using the Density-Based Spatial Clustering of Applications with Noise（DBSCAN）algorithm. The developed CNN model, demonstrating a 98.32% accuracy rate in validation, effectively discriminated between the signals corresponding to distinct stages of material damage. This research underlines the efficacy and practicality of integrating AE monitoring with deep learning for hydrogen induced damage detection in materials.

Keywords: Hydrogen Embrittlement; Acoustic Emission Monitoring; Deep Learning; Austenitic Stainless Steel; DBSCAN Algorithm; CNN Model

1. INTRODUCTION

Hydrogen, as a clean energy source, demonstrates immense potential in addressing global energy crises and reducing environmental pollution. In recent years, with the advancement of hydrogen technology, hydrogen's applications in energy storage, transportation, and as a fuel have expanded rapidly. However, these applications pose a significant materials science challenge: hydrogen embrittlement [1]. Hydrogen embrittlement refers to the phenomenon where the toughness and strength of metals and alloys significantly decrease in environments with hydrogen gas or internal hydrogen atom penetration [2]. This phenomenon is particularly crucial in high-pressure hydrogen environments

© 2024 by ASME

and can lead to unexpected failures in critical structures like pipelines and pressure vessels, causing substantial economic losses and safety hazards.

Research on hydrogen embrittlement began in the early 20th century, initially focusing on steel and other traditional metal materials [3-4]. Over time, researchers found that hydrogen embrittlement also significantly impacts high-performance alloys, such as austenitic stainless steel. Due to its excellent mechanical properties and corrosion resistance, austenitic stainless steel is widely used in fields like chemical, nuclear, and marine engineering [5-6], especially important in hydrogen transportation and storage.

In recent years, scientists have been striving to gain a deeper understanding of hydrogen embrittlement, particularly its impact on austenitic stainless steel. On one hand, advanced experimental techniques like Transmission Electron Microscopy (TEM) and Scanning Electron Microscopy (SEM) have allowed researchers to observe the process of hydrogen-induced crack formation at the micro level. On the other hand, theoretical models and computational methods have been used to predict and explain the mechanisms of hydrogen embrittlement [7-8]. These studies provide crucial guidance for improving the design and treatment of austenitic stainless steel.

Despite these advancements, the detection of hydrogen embrittlement remains a challenge [9-10]. According to API 510 standards, regular inspections and tests of hydrogen equipment are typically conducted through hydrostatic testing complemented by traditional non-destructive testing procedures [11-12]. However, these methods cannot detect damage during equipment operation. During material deformation, a phenomenon known as AE occurs, where elastic stress waves are released due to the accumulation of energy [13]. Over the past few decades, AE in-situ monitoring technology has been proven to effectively detect hydrogen damage in materials [14]. The application of AE technology offers a new solution to this problem [15-16]. AE is a non-destructive testing technique that can monitor microcracks and damage within materials in real-time. Advanced analysis methods, such as CNN, can be used to conduct deeper analysis of collected AE signals, allowing for timely and accurate identification of material changes caused by hydrogen embrittlement. Toubal et al. [17-18] used the AE method to study the crack formation caused by stress concentration during hydrogen diffusion tests. They discovered stress concentration during the hydrogen diffusion process and discussed the use of AE methods for hydrogen embrittlement detection. Qiu Feng et al. [19] used the AE method to study the damage mechanisms and characteristics of hydrogen reactors. Additionally, for the identification of hydrogen damage characteristics based on AE, traditional machine learning methods rely on manual experience for feature extraction. The optimization of feature design, feature extraction, and model training cannot be combined [20].

Existing studies often involve repetitive removal and reinstallation of samples during signal collection to interpret the acoustic signals, a process that is cumbersome and prone to introducing experimental inconsistencies [21-22]. This research proposes using an unsupervised machine learning clustering algorithm to categorize AE signals collected throughout the experiment, offering a new approach in selecting datasets for damage recognition models using deep learning.

2. EXPERIMENTAL CONDITIONS

The study was repeated three times under the same conditions, it utilized 304 austenitic stainless steel to prepare the samples [23], the composition of 304 austenitic stainless steel is as shown in Table 1. As depicted in Figure 1, the samples were rectangular iron bars with 200 mm in length, 20 mm in width, and 3 mm in thickness. The samples, which include a holding section transitioning to a parallel section via an arc, were sanded and polished with sandpaper and polishing wheels on the surface of the blanks to a surface roughness of 4. They were then subjected to high-pressure hydrogen charging at 300°C and 20 MPa for five days.

AE monitoring was conducted using two NANO-30 GO34 type miniature sensors linearly arranged on the samples, closely contacting them through a coupling agent. The sensor locations are illustrated by the blue circles in Figure 1. Each sensor has a monitoring range of 10 cm, so changes in the AE signal at all positions of the specimen can be monitored. The sensor outputs, amplified by a preamplifier with a 40dB gain, were fed into a computer for data recording and monitoring.

Instron hydraulic tensile testing machines were employed for loading the samples. Pre-stretching at low stress eliminated friction between the sample holding sections and the testing machine. During the actual stretching experiment, with a strain rate of 5×10^-5 mm/s, AE signals were continuously monitored, as shown in Figure 2.

TABLE 1: CHEMICAL COMPOSITION OF THE 304 AUSTENITIC STAINLESS STEEL USED

	C	Si	Mn	P	S	Ni	Cr	Fe
Type 304	0.05	0.61	1.56	0.04	0.024	8.55	18.2	Balanced

© 2024 by ASME

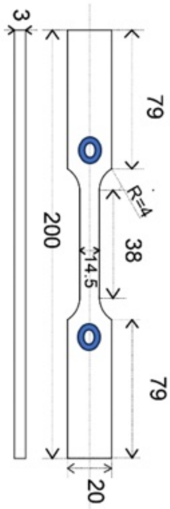

FIGURE 1: SPECIMEN SIZE AND SENSOR LOCATION

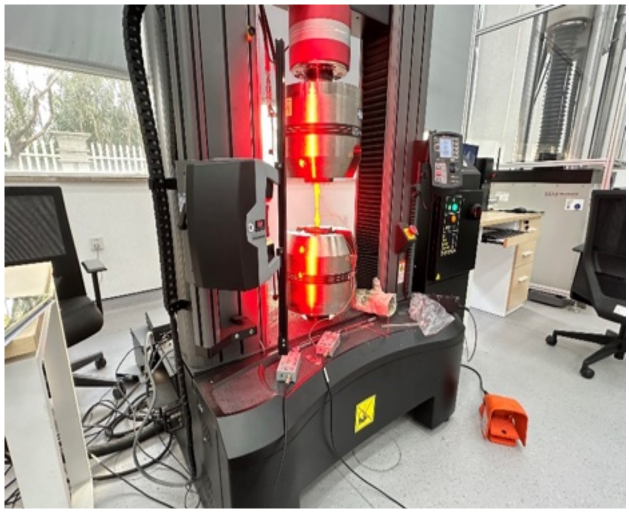

FIGURE 2: EXPERIMENTAL ASSEMBLY

Before collecting AE signals, a 15-20 minute background noise measurement was performed to set a fixed threshold for the AE monitoring software. The software parameters are detailed in Table 2, using a sampling rate of two Million Samples Per Second (MSPS), the Peak Definition Time (PDT) is 300 microseconds, the Hit Definition Time (HDT) is 600 microseconds, and the Hit Lockout Time (HLT) is 1000 microseconds. After the samples were stretched at a constant rate until rupture, the AE signals collected throughout the stretching experiment were saved for further analysis.

TABLE 2: SET-UP OF AE PARAMETER

Fixed thresholds/ dB	Sample rate	Pre-triggered	length	AE parameter settings			Maximum duration/(µs).
				PDT (µs)	HDT (µs)	HLT (µs)	
35	2MSPS	128	2k	300	600	1000	1000

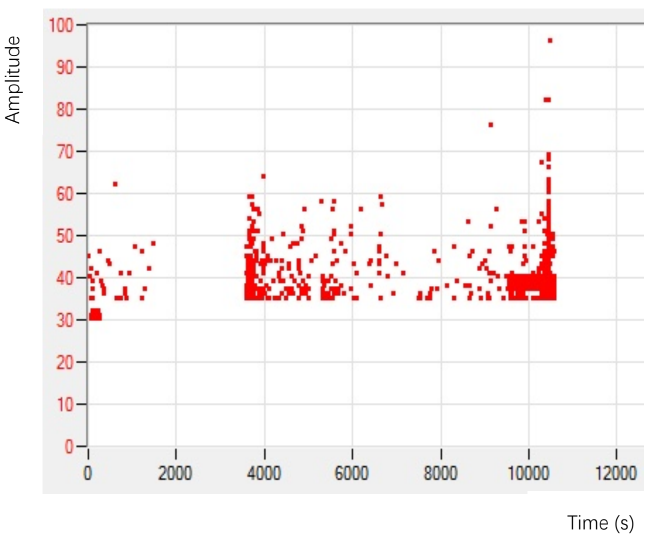

FIGURE 3: VARIATION OF AMPLITUDE WITH TIME

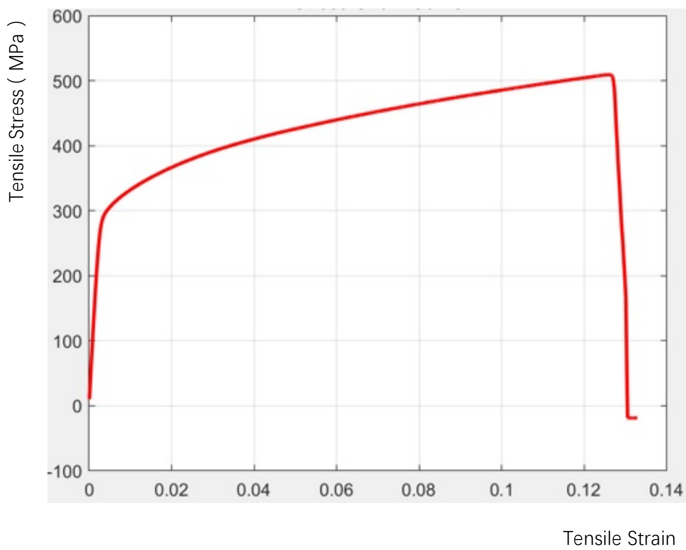

FIGURE 4: HYDROGEN-PRECHARGED SPECIMEN STRESS-STRAIN CURVE

© 2024 by ASME

3. RESULTS

3.1 Analysis and Processing of Acoustic Emission Signals

We show the process of analyzing the results of one set of experiments as an example. The study began recording AE signals from 10,000 seconds, corresponding to the curve inflection point in Figure 4, marking the onset of the necking stage and the initiation of cracks, evident from the significant increase in the number and amplitude of AE signal points in Figure 3. At the moment of material fracture, the amplitude of AE signals peaked. Analysis of Figure 5 revealed that the fracture location was near Sensor 2, corroborating the data shown in Figure 6, where a high number and amplitude of AE points were observed near the coordinates of Sensor 2.

A comprehensive analysis revealed that AE signals during material fracture exhibit characteristics such as a sudden increase in frequency and amplitude, reflecting rapid energy release; an increase in signal amplitude due to material failure; higher frequency components due to the rapid propagation of cracks; and the localization of AE sources primarily near the area where fracture is imminent.

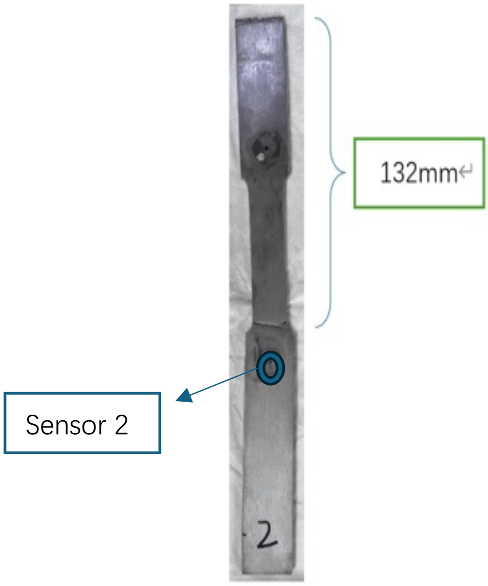

FIGURE 5: HYDROGEN-PRECHARGED SPECIMEN FRACTURE

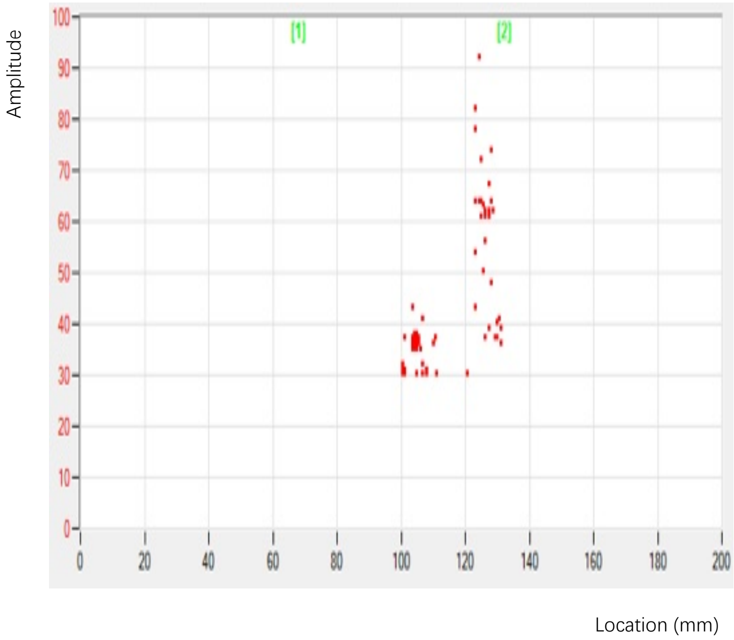

FIGURE 6: VARIATION OF AMPLITUDE IN LOCATION

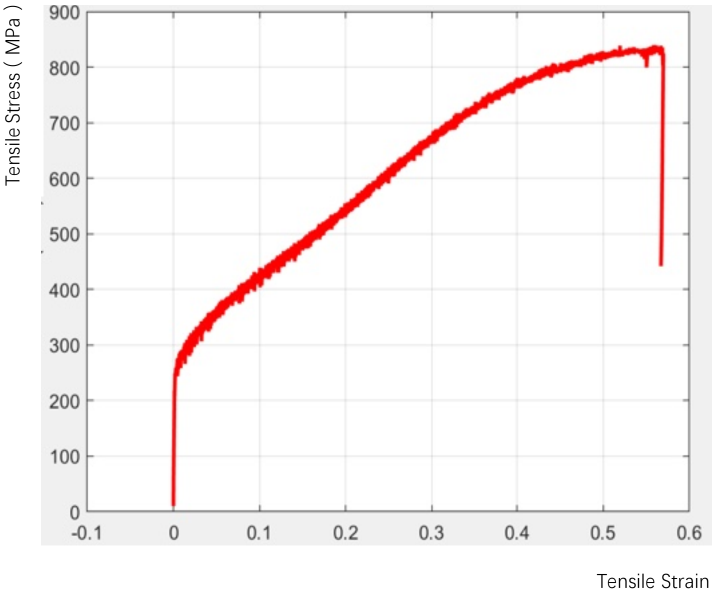

FIGURE 7: NON-HYDROGEN-CHARGED SPECIMEN STRESS-STRAIN CURVE

FIGURE 8: NON-HYDROGEN-CHARGED SPECIMEN FRACTURE

© 2024 by ASME

3.2 Comparison of Tensile Curves between Hydrogen-Precharged Samples and Non-Hydrogen-Charged Samples

Two sets of tensile tests were performed on non-precharged hydrogen specimens of the same size under the same experimental conditions. One set was taken as an example for analysis. Comparing Figures 4 and 7, it is observed that the tensile strain at fracture for the non-hydrogen-charged samples is approximately five times that of the hydrogen-precharged samples. Additionally, an analysis of Figures 5 and 8 reveals that the length of the non-hydrogen-charged samples after fracture is greater than that of the hydrogen-precharged samples.

In order to quantitatively compare the effect of hydrogen concentration in the specimen on the tensile strain, we took a 10mm × 10mm × 3mm square from the hydrogen-precharged sample that had undergone tensile test for Total Dissolved Solids (TDS) testing, and used HIDEN TPD Workstation to measure the hydrogen concentration for 5.72h under a starting temperature of 20 degrees Celsius and a vacuum level of 10^{-10} times the standard atmospheric pressure. The Mass Spec Response-Elapsed Time graph line was Figure 9, we obtained the mass of hydrogen in the cube of 4.72×10^{-5}g. The cube was weighed (Figure 10 for calculating hydrogen concentration of the specimen) to give the mass of 1.9651 g. The hydrogen concentration of the specimen was calculated to be 24 parts per million (ppm), the formula is $\frac{m(H_2)}{m(cube)}\times10^{6}$.

The toughness was derived by calculating the area under the stress-strain curve, we got that the toughness of the non-precharged hydrogen specimen was 353.87MPa, and the toughness of the hydrogen-precharged specimen was 55.52MPa. We can calculate the proportion of toughness reduction, the formula is the proportion of toughness reduction $= \left(1-\frac{Toughness\ of\ the\ hydrogenated\ specimen}{Toughness\ of\ unhydrogenated\ specimen}\right)\times100\%$. According to the calculation, the toughness of the specimen with hydrogen content of 24 ppm is reduced by about 84.31%. This indicates that the strain of the hydrogen-precharged specimen in the tensile experiment is drastically reduced compared to the non-precharged hydrogen specimen, reflecting a significant reduction in toughness. This significant reduction in toughness points to the strong negative impact of hydrogen embrittlement on material properties.

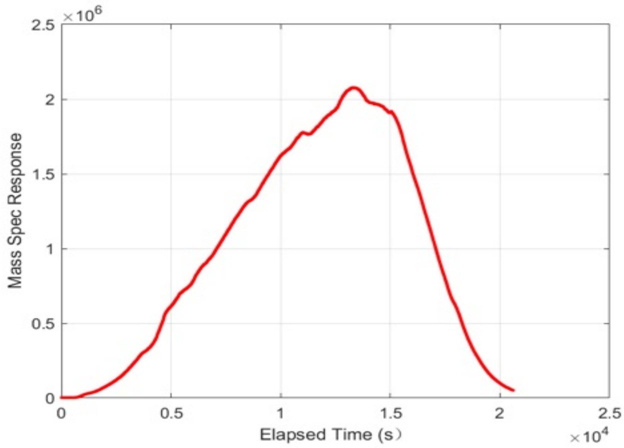

FIGURE 9: MASS SPEC RESPONSE-ELAPSED TIME CURVE

FIGURE 10: CUBE WEIGHING

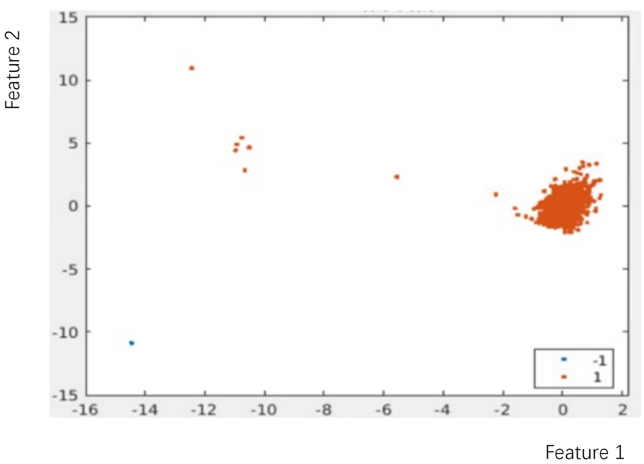

FIGURE 11: DBSCAN CLUSTERING EFFECT OF INTENSIFICATION PHASE

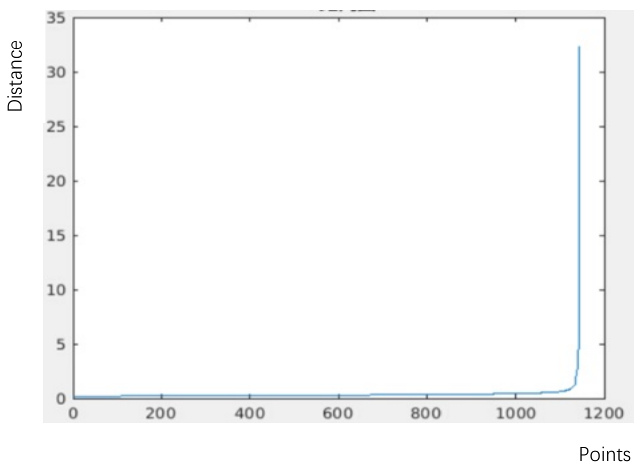

FIGURE 12: K-DISTANCE DIAGRAM OF INTENSIFICATION PHASE

© 2024 by ASME

3.3 Unsupervised Clustering of Acoustic Emission Signals

In our study, we use the MATLAB language to address the signal data from the audio file to perform the short time Fourier transform. The Short-Time Fourier Transform is a signal processing technique used to analyze frequency and phase changes over time. Unlike the traditional Fourier Transform (FT), the STFT splits the signal into small segments and then performs a Fourier Transform on each small segment to be able to observe the change in the frequency components of the signal at different points in time. In this way, the STFT can provide information about the signal in both time-frequency dimensions, helping to understand the local characteristics of the signal. Every 2048 data points were taken as a signal sample, after multiple iterations of experiments, it was determined that a sliding window size of 164 samples and a stride length of 41 samples can effectively reflect the local characteristics of the signal, and then standardized the STFT result.

We conducted a clustering analysis on the STFT results of the acoustic emission signals, The study utilized the DBSCAN algorithm for unsupervised clustering of AE signals processed through STFT. DBSCAN excels in handling clusters of various shapes and sizes and demonstrates robustness against noise. Unlike centroid-based algorithms like K-means, DBSCAN does not require prior knowledge of the number of clusters, making it effective for complex datasets and outlier detection. DBSCAN's application spans various industries, including seismology and ecology.

In DBSCAN, a point's density is defined by the number of points within its ε-neighborhood. A point becomes a core point if at least minPts other points are within its ε-neighborhood, indicating a high-density area. Border points, although not core points themselves, are within the ε-neighborhood of a core point. Points not qualifying as either core or border points are considered noise. The algorithm clusters core points and their density-reachable points (including other core points and border points). Clusters merge if a core point is density-reachable from another core point, allowing clusters to grow in size and shape.

For the STFT results, a zero matrix was initially allocated to store features of all files. Each file was processed in a parallel loop, calculating spectral centroid, band energy ratio, spectral entropy, and average brightness of the STFT histogram. Features were standardized to zero mean and unit variance. Epsilon (ε) and minPts were determined to establish the clustering model, with epsilon defining the maximum distance for points to be considered neighbors and minPts set as the number of points required in a neighborhood to define a core point. K-nearest neighbors search calculated the k-distance for each point, and a k-distance graph was plotted. The epsilon value was chosen from the "elbow" of the k-distance graph (the point of maximum curvature), with minPts set to one more than the number of features. Following these steps, DBSCAN clustering was performed, and scatter plots visualized the results.

We focused particularly on two distinct stages: the initial half of the hardening phase and the transition from the late hardening to the necking stage, to determine the appropriate parameters for the DBSCAN algorithm in these stages, we first plotted k-distance graphs (as shown in Figures 12 and 14). Given that the feature count was four, we set the minPts parameter to 5, one more than the number of features. With these parameters, we executed the DBSCAN algorithm and created scatter plots (illustrated in Figures 11 and 13) to visualize the clustering outcomes.

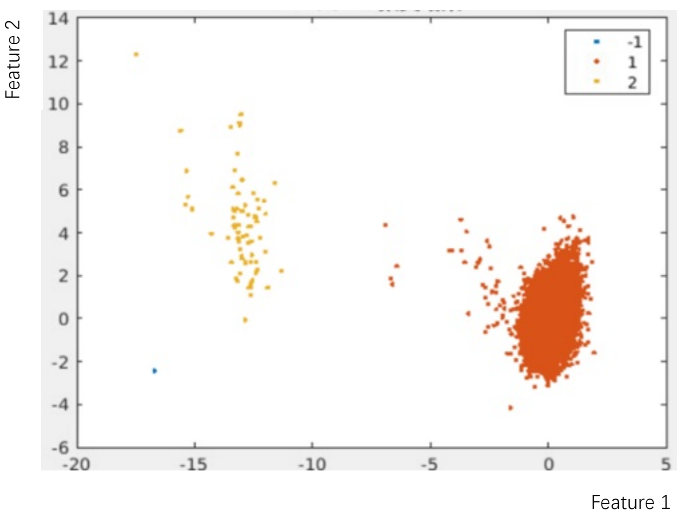

FIGURE 13: DBSCAN CLUSTERING EFFECT OF EVENING OF THE INTENSIFICATION PHASE TO THE NECK-DOWN PHASE

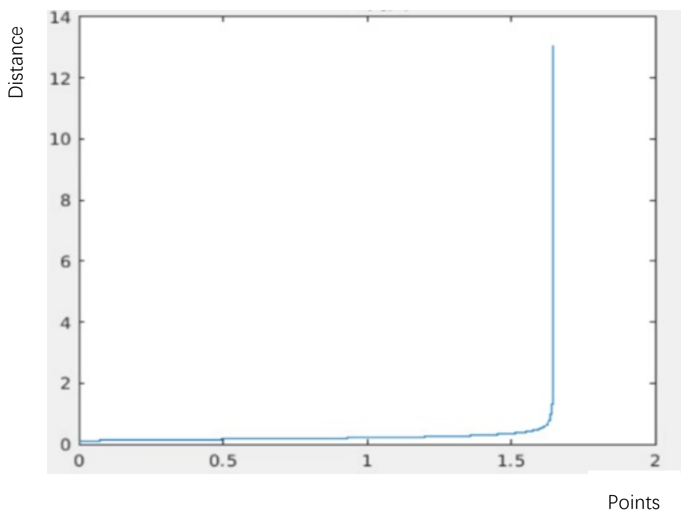

FIGURE 14: K-DISTANCE DIAGRAM OF EVENING OF THE INTENSIFICATION PHASE TO THE NECK-DOWN PHASE

© 2024 by ASME

Analyzing Figures 11 and 13, Feature 1 represents the spectral center of mass, which is obtained by calculating the weighted average of all frequency components, where the weights are the amplitudes of the corresponding frequency components. The spectral center of gravity can indicate the location of the "center of gravity" of the signal spectrum and is usually associated with the perceived brightness of the signal. Feature 2 is the ratio of the energy in the first quarter of the calculated frequency range to the energy of the entire spectrum, and this ratio reflects the distribution of signal energy in a particular frequency band. Label -1 denotes noise points, label 1 and label 2 denote different clustering labels, and each number represents a different cluster of clusters. A distinct clustering pattern was observed in the initial half of the hardening stage, characterized by a prominent cluster of red points on the right side in Figure 11. In contrast, during the late hardening to necking transition, two separate clusters emerged: a cluster of yellow points on the left and a cluster of red points on the right in Figure 13. A comparison of the central coordinates of the red clusters in both figures revealed their proximity to the (0,0) coordinate, indicating similarity in the signal types. The presence of the yellow cluster primarily in the later stage suggests its association with crack signals. In summary, it can be obtained that label 1 is the normal structure data label and label 2 is the cracked structure data label.

Additionally, during the late strengthening phase to the necking stage of the specimen stretching process, we conducted Industrial CT(SANYING-TS20131) inspection and X-ray digital imaging inspection from different directions and angles, four times each. The X-ray digital imaging inspection had a maximum tube voltage of 225 kV, a spatial resolution of ≤ 2 μm, a density resolution of ≤ 2%, and used a flat panel detector measuring 430 mm × 430 mm. As illustrated in Figure 15, CT provided multi-angular confirmation of the existence of a singular principal crack during the late strengthening phase to the necking stage. This discovery aligns with the crack type identified through unsupervised clustering analysis of STFT-processed AE signals using the DBSCAN algorithm. The multi-dimensional images obtained from CT scanning at different angles not only verified the presence of this principal crack but also enhanced the precision and reliability of the AE monitoring method. This synergistic use of CT imaging and AE signal analysis offers a reliable approach for verifying and understanding the crack patterns and their progression in the material under study.

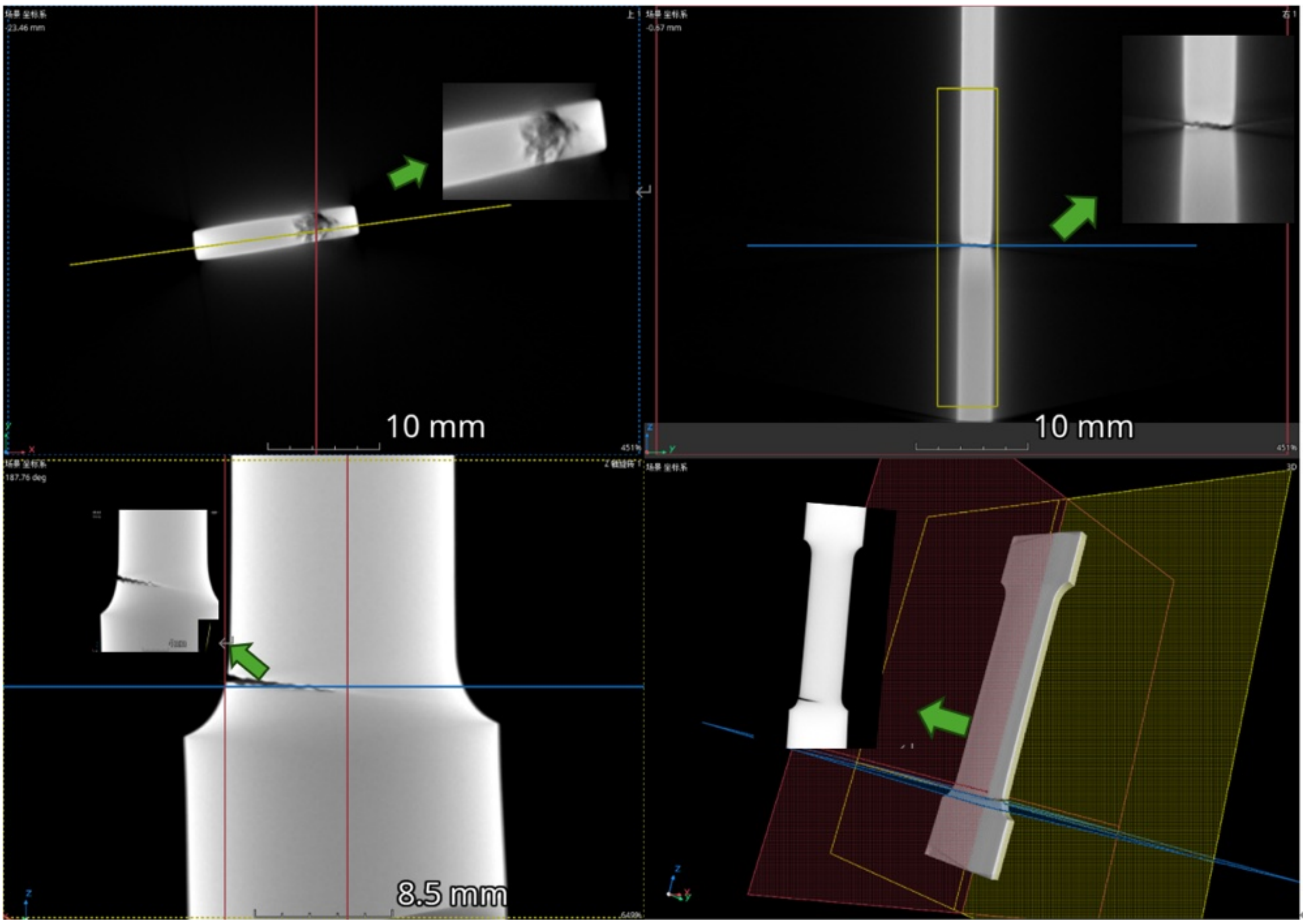

FIGURE 15: INDUSTRIAL CT IMAGE OF THE HYDROGEN-PRECHARGED SAMPLE CRACK EXPANSION

© 2024 by ASME

3.4 Convolutional Neural Network Model

We did three sets of tensile experiments on hydrogen-precharged specimens in the same experimental environment and experimental conditions, and processed the collected data as described above to train the STFT results using a CNN framework. CNNs are highly effective in audio processing and classification, particularly with STFT data in MAT format, the MAT format is a file format used by MATLAB software to store variables and data within MATLAB.

CNN's convolutional layers extract local features from STFT data, akin to edges and textures in images. Convolution kernels slide over the STFT matrix, extracting spectral feature information. The following pooling layers reduce the feature map size while retaining essential information, lowering computational complexity and enhancing the model’s generalizability. Convolution and pooling layers are usually followed by fully connected layers that map the extracted audio features to the final output categories. Activation functions are applied after convolution and fully connected layers, with loss functions measuring model performance and prediction error. During training, weights and parameters are adjusted through backpropagation to minimize the loss function.

The STFT results, a complex number two-dimensional array sized 128x61, were visualized in terms of magnitude, converting them into a real-number matrix for further processing. Using MATLAB's deep learning toolbox to construct the CNN model, the input data format required was [height, width, channels, samples]. The original data, a two-dimensional matrix, was first transposed (data'), then reshaped to new dimensions of 61 (width), 128 (height), 1 (channel), and the number of samples. The data_4D array dimensions were rearranged using the permute function, changing the dimension order from [61, 128, 1, numSamples] to [128, 61, 1, numSamples] to match MATLAB's standard image data format.

The CNN model comprised two convolutional layers, each followed by a batch normalization layer and a ReLU activation layer. These convolutional layers utilized 3x3 filters to extract features, with the first layer having 8 output channels and the second increasing to 16. Batch normalization layers after each convolutional layer accelerated training and enhanced model stability, while ReLU layers introduced the necessary non-linearity. Two max pooling layers with 2x2 windows reduced the feature map size, preserving vital information. The fully connected layer mapped learned features to the output space of the classification task, followed by a softmax layer converting outputs to probability distributions. Finally, the classification layer outputted the model's decisions.

The CNN was trained using the Adam optimizer, which adapts the learning rate. The initial learning rate was set at 0.001, balancing training speed with convergence stability. Training was planned to complete within 20 epochs, each representing a full pass through the entire dataset. To prevent overfitting, the data were shuffled before each epoch. Additionally, the model's performance was evaluated on an independent test set every 30 iterations, continuously monitoring and validating the learning process.

Labels were created for two data categories: intact structure (labelled 0) and crack (labelled 1). The data were divided into training set (64% for model training), validation set (16% for testing model accuracy while training) and test set (20% for testing model accuracy after training). The model was validated using the signals from the test set to observe how the experimental results of the proposed approach performed. The accuracy of the model recognition is the ratio of the correct number of samples to the total number of samples. The experimental performances of the models presented in this paper were assessed using this accuracy calculation method.

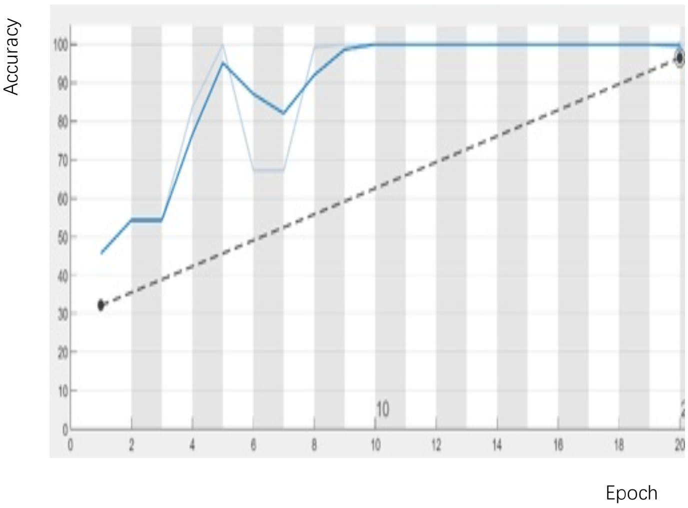

FIGURE 16: ACCURACY DURING TRAINING

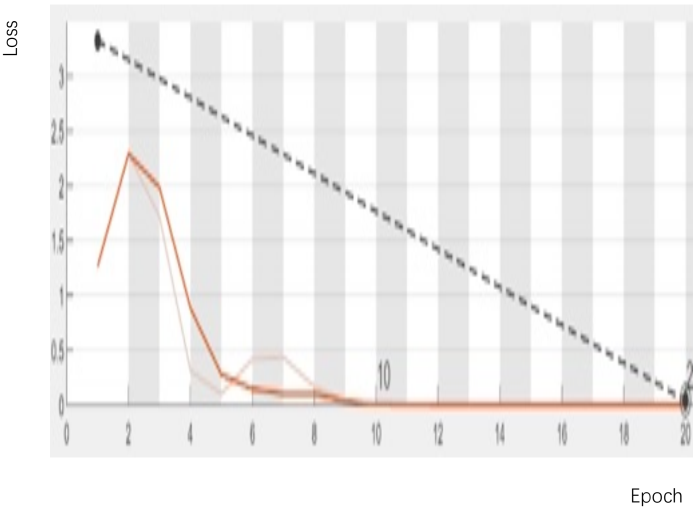

FIGURE 17: LOSS DURING TRAINING

© 2024 by ASME

Analysis of Figures 16 and 17 revealed an improvement in model performance as training progressed. Model accuracy, represented by the blue line, showed an overall upward trend with increasing iterations, particularly in the latter stages of training. The final validation accuracy reached approximately 98.32%, indicating a significant enhancement in the model's predictive capabilities. Concurrently, the loss value, depicted by the orange line, initially increased and continued to fluctuate throughout the training process, yet displayed an overall downward trajectory. This pattern suggests that the model was effectively learning and refining its predictions over time.

Notably, the consistent decrease in the loss value and the absence of an upward trend in this metric imply that the model did not suffer from overfitting. The model's performance on the validation set did not deteriorate due to excessive adaptation to the training data. Additionally, the smooth increase in the accuracy curve suggests an improvement in the model's generalization ability. These observations confirm that the developed CNN model effectively learned and predicted features in the STFT data, demonstrating robust classification performance.

4. CONCLUSION

This comprehensive study presents a novel approach to understanding the behavior of 304 austenitic stainless steel under hydrogen embrittlement conditions. The research employed AE monitoring in conjunction with a CNN to analyze the material's response to stress and potential damage. The use of AE monitoring, a real-time non-destructive testing technique, was instrumental in detecting changes in sound wave signals during the material's stress phases, particularly in critical stages like necking and crack formation [24].

The study's innovative aspect lies in its integration of AE monitoring with advanced machine learning techniques. By using the DBSCAN algorithm for unsupervised clustering of STFT processed AE signals, the research was able to effectively differentiate signals corresponding to various damage stages. This method provides a more nuanced understanding of the material's behavior under stress, offering a critical tool in damage detection and assessment.

The CNN model with a multi-layered structure extracted fundamental features from the STFT data and accurately classified them. The model was validated using signal data from the test set, observing its recognition accuracy on the new dataset, with a validation accuracy reaching as high as 98.32%. CNN models excel at identifying patterns and features in complex data, hence they have the potential to capture the characteristics of crack nucleation from similar signals provided by both sensors. Notably, the model demonstrated robustness, showing no signs of overfitting, which underscores its potential for practical applications.

With respect to the issue of specimen fracture in the non-standard distance region, we recognize that this phenomenon stems primarily from the design of the specimen transition section being too short, resulting in stress concentrations. This design limitation may have affected the desirability of the experimental results, but we would like to emphasize that the validity of our data analysis methodology and associated algorithms has not been compromised despite this problem. By accurately distinguishing between cracked and normal structure data, our analysis was still able to provide critical material property information, and in particular showed significant value in determining the type of hydrogen damage. We plan to further optimize the specimen design in subsequent studies, especially by extending the transition section to reduce stress concentration effects. And we believe that these improvements will significantly enhance the accuracy of the experiments and the reliability of the results. In addition, we will also consider adopting more diverse materials and more advanced data analysis techniques to deepen our understanding of hydrogen damage behavior and validate our research results.

In conclusion, this study represents a step forward in the field of material science and engineering [25-26]. It demonstrates the potential of integrating AE monitoring with CNNs and unsupervised clustering algorithms for effective material damage detection and analysis. While acknowledging its limitations, the study paves the way for future research that could further refine and enhance these techniques, ultimately contributing to offering a proactive approach to material failure prevention and risk management, safer and more efficient industrial practices.

5 ACKNOWLEDGEMENTS

This research was supported by the National Key Research and Development Program of China (Grant No. 2022YFB4003400), China Scholarship Council (Grant No. 202106320138), State Key Laboratory of Clean Energy Utilization and Zhejiang University K.P.Chao’s High Technology Development Foundation, China

 © 2024 by ASME

REFERENCES

[1] Qiu, F., Shen, Z., Bai, Y., Shan, G., Qu, D., & Chen, W. (2022). Hydrogen defect acoustic emission recognition by deep learning neural network. State Key Laboratory of Safety and Control for Chemicals, SINOPEC Research Institute of Safety Engineering Co., Ltd, Qingdao, 266000, China.

[2] Cho, H., & Takemoto, M. (2007). Hydrogen related brittle cracking of metastable type-304 stainless steel. Faculty of Science and Engineering, Aoyama Gakuin University, 5-10-1 Fuchinobe, Sagamihara, Kanagawa 229-8558, Japan.

[3] Alvarez, M. G.*, Lapitz, P., & Ruzzante, J. (2008). AE response of type 304 stainless steel during stress corrosion crack propagation. Comisión Nacional de Energía Atómica, Centro Atómico Constituyentes, Avda. Gral. Paz 1499, 1650 San Martín, Prov. Buenos Aires, Argentina; Agencia Nacional de Promoción Científica y Tecnológica, Comisión Nacional de Energía Atómica, CAC, Avda. Gral. Paz 1499, 1650 San Martin, Prov. Buenos Aires, Argentina; Universidad Tecnológica Nacional, Facultad Regional Delta, Argentina. doi:10.1016/j.corsci.2008.08.02

[4] W.W. Gerberich, R.H. Jones, M.A. Friesel, A. Nozue, Acoustic emission monitoring of stress corrosion cracking, Mater. Sci. Eng. A103 (1988) 185–191.

[5] M. Y. Maeda, M. Koyama, H. Nishimura, et al., Hydrogen-assisted damage evolution in nitrogen-doped duplex stainless steel, Int. J. Hydrogen Energ. 46(2021) 2716-2728. https://doi.org/ 10.1016/j.ijhydene.2020.10.152.

[6] B. Cox, A correlation between acoustic emission and fractography of cracking during SCC of zircaloys, Corrosion 30 (1974) 191–202.

[7] T. K. Mandal, V. P. Nguyen, J. Y. Wu, Comparative study of phase-field damage models for hydrogen assisted cracking, Theor. Appl. Fract. Mec. 111 (2021) 102840. https://doi.org/ 10.1016/j.tafmec.2020.102840.

[8] M. Abreu, M. Iordachescu, A. Valiente, On hydrogen-induced damage in cold-drawn lean-duplex wires, Eng. Fail. Anal. 91 (2018) 516-526. https://doi.org/ 10.1016/j.engfailanal.2018.04.036.

[9] K. Darowicki, A. Mirakowski, S. Krakowiak, Investigation on pitting corrosion of stainless steel by means of acoustic emission and potentiodynamic methods, Corros. Sci. 45 (2003) 1747–1756. steel exhibiting varying ductility, J. Mater. Sci and Eng, 486 (2008) 562-571.

[10] H. Roy, N.Parida, S. Sivaprasad, S. Tarafder, K.K Ray, Acoustic emissions during fracture toughness tests of steel exhibiting varying ductility, J. Mater. Sci and Eng, 486 (2008) 562-571.

[11] Z. Kral, W. Horn, J. Steck, Crack propagation analysis using acoustic emission sensors for structural health monitoring system, The Scientific World Journal, 2013 (2013) 1-13.

[12] Z. Han, H. Lou, H. Wang, Effect of strain rate and notch on acoustic emission during the tensile deformation of a discontinuous yielding material, J. Mater Sci and Eng. 528 (2011) 4372-4380.

[13] T. K. Mandal, V. P. Nguyen, J. Y. Wu, Comparative study of phase-field damage models for hydrogen assisted cracking, Theor. Appl. Fract. Mec. 111 (2021) 102840. https://doi.org/ 10.1016/j.tafmec.2020.102840.

[14] M. Abreu, M. Iordachescu, A. Valiente, On hydrogen-induced damage in cold-drawn lean-duplex wires, Eng. Fail. Anal. 91 (2018) 516-526. https://doi.org/ 10.1016/j.engfailanal.2018.04.036.

[15] S. J. Yoon, H. J. Lee, K. B. Yoon, et al. Hydrogen damage in 34CrMo4 pressure vessel steel with high tensile strength, J. Mech. Sci. Technol. 32 (2018) 637-646. https://doi.org/ 10.1007/s12206-018-0111-7.

[16] Y. Sun, Y. F. Cheng, Hydrogen permeation and distribution at a high-strength X80 steel weld under stressing conditions and the implication on pipeline failure, Int. J. Hydrogen Energ. 46 (2021) 23100-23112. https://doi.org/10.1016/j.ijhydene.2021.04.115.

[17] L. F. Li, Z. Zhang, G. T. Shen, et al., Acoustic emission as a technique to study hydrogen induced cracking behavior of low-carbon steel, IEEE, 2010. https://doi.org/10.1109/CISP.2010.5647796.

[18] L. Toubal, H. Chaabouni, P. Bocher, et al., Monitoring fracture of high-strength steel under tensile and constant loading using acoustic emission analysis, Eng. Fail. Anal. 108 (2020) 104260.

[19] E. D. Merson, M. M. Krishtal, D. L. Merson, et al. Effect of strain rate on acoustic emission during hydrogen assisted cracking in high carbon steel. Mat. Sci. Eng. A 550 (2012) 408-417.

[20] G. Serin, B Sener., A. M. Ozbayoglu, et al., Review of tool condition monitoring in machining and opportunities for deep learning, Int. J. Adv. Manuf. Tech. 109 (2020) 953-974. https://doi.org/10.1007/s00170-020-05449-w.

[21] T. Shiraiwa, M. Kawate, F. Briffod, et al., Evaluation of hydrogen-induced cracking in high-strength steel welded joints by acoustic emission technique, Mater. Design 190 (2020) 108573.

© 2024 by ASME

[22] M. Szymanski, J. Plowiec, B. Michalski, et al., Monitoring of the hydrogen decrepitation process by acoustic emission, Solid State Sci. 89 (2019) 106-113. https://doi.org/10.1016/j.matdes.2020.108573.

[23] D. Wang, B. Liao, C. Hao, et al., Acoustic emission characteristics of used 70 MPa type IV hydrogen storage tanks during hydrostatic burst tests, Int. J. Hydrogen Energ. 46 (2021) 12605-12614. https://doi.org/10.1016/j.ijhydene.2020.12.177.

[24] E. D. Merson, P. N. Myagkikh, G. V. Klevtsov, et al., Effect of fracture mode on acoustic emission behavior in the hydrogen embrittled low-alloy steel, Eng. Fract. Mech. 210 (2019) 342-357. https://doi.org/10.1016/j.engfracmech.2018.05.026.

[25] T. T. Nguyen, H. M. Heo, J. Park, et al., Damage assessment and mechanical performance of Cr-Mo steel used in hydrogen storage vessels, Eng. Fail. Anal. 120 (2021) 105031. https://doi.org/ 10.1016/j.engfailanal.2020.105031.

[26] N. Munir, H.J. Kim, J. Park, S.J. Song, S.S. Kang, Convolutional neural network for ultrasonic weldment flaw classification in noisy conditions, Ultrasonics 94 (2018) https://doi.org/10.1016/j.ultras.2018.12.001

© 2024 by ASME

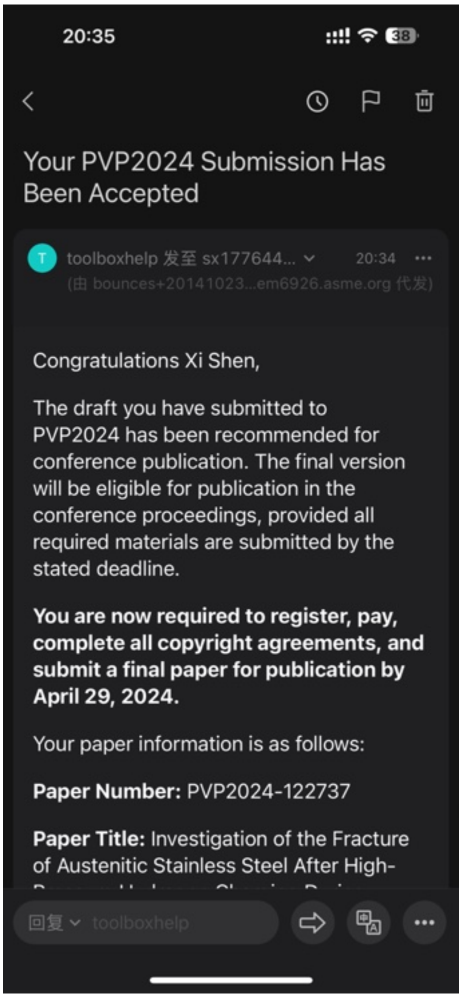

20:35

Your PVP2024 Submission Has Been Accepted

toolboxhelp 发至 sx177644... 20:34

(由 bounces+20141023...em6926.asme.org 代发)

Congratulations Xi Shen,

The draft you have submitted to PVP2024 has been recommended for conference publication. The final version will be eligible for publication in the conference proceedings, provided all required materials are submitted by the stated deadline.

You are now required to register, pay, complete all copyright agreements, and submit a final paper for publication by April 29, 2024.

Your paper information is as follows:

Paper Number: PVP2024-122737

Paper Title: Investigation of the Fracture of Austenitic Stainless Steel After High-

回复 toolboxhelp

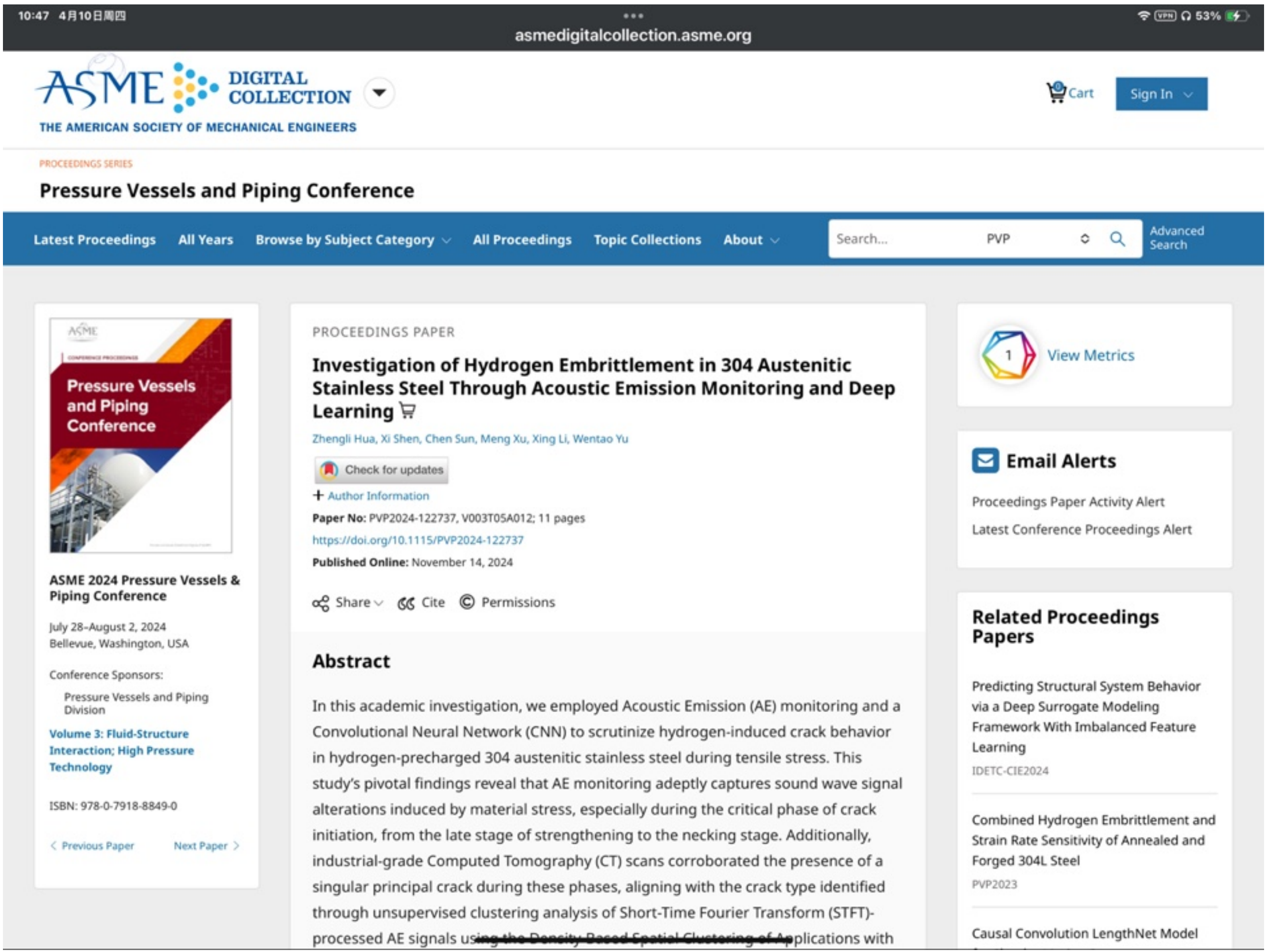

10:47 4月10日周四

asmedigitalcollection.asme.org

ASME DIGITAL COLLECTION

THE AMERICAN SOCIETY OF MECHANICAL ENGINEERS

Cart Sign In

PROCEEDINGS SERIES

Pressure Vessels and Piping Conference

Latest Proceedings | All Years | Browse by Subject Category | All Proceedings | Topic Collections | About | Search... PVP | Advanced Search

Pressure Vessels and Piping Conference

ASME 2024 Pressure Vessels & Piping Conference

July 28–August 2, 2024

Bellevue, Washington, USA

Conference Sponsors:

Pressure Vessels and Piping Division

Volume 3: Fluid-Structure Interaction; High Pressure Technology

ISBN: 978-0-7918-8849-0

Previous Paper | Next Paper

PROCEEDINGS PAPER

Investigation of Hydrogen Embrittlement in 304 Austenitic Stainless Steel Through Acoustic Emission Monitoring and Deep Learning

Zhengli Hua, Xi Shen, Chen Sun, Meng Xu, Xing Li, Wentao Yu

Check for updates

+ Author Information

Paper No: PVP2024-122737, V003T05A012; 11 pages

https://doi.org/10.1115/PVP2024-122737

Published Online: November 14, 2024

Share | Cite | Permissions

Abstract

In this academic investigation, we employed Acoustic Emission (AE) monitoring and a Convolutional Neural Network (CNN) to scrutinize hydrogen-induced crack behavior in hydrogen-precharged 304 austenitic stainless steel during tensile stress. This study's pivotal findings reveal that AE monitoring adeptly captures sound wave signal alterations induced by material stress, especially during the critical phase of crack initiation, from the late stage of strengthening to the necking stage. Additionally, industrial-grade Computed Tomography (CT) scans corroborated the presence of a singular principal crack during these phases, aligning with the crack type identified through unsupervised clustering analysis of Short-Time Fourier Transform (STFT)-processed AE signals us~~ing the Density-Based Spatial Clustering of A~~pplications with

View Metrics

Email Alerts

Proceedings Paper Activity Alert

Latest Conference Proceedings Alert

Related Proceedings Papers

Predicting Structural System Behavior via a Deep Surrogate Modeling Framework With Imbalanced Feature Learning

IDETC-CIE2024

Combined Hydrogen Embrittlement and Strain Rate Sensitivity of Annealed and Forged 304L Steel

PVP2023

Causal Convolution LengthNet Model

© 2024 by ASME

项目名称：纯氢与天然气掺氢长输管道输送及应用关键技术(项目编号:2022YFB4003400)

委托单位：中石化新星(北京)新能源研究院有限公司

合同金额（经费预算）：总需求 6485.00 万元，其中中央财政专项资金需求 785.00 万元

本人排名：沈曦（35）

项目主要研究内容：

任务 1:纯氢管道输送应用验证及科技试验平台

针对研究课题 1-4 研发的长输管道输送及应用关键技术，制定纯氢管道平台建设方案，搭建纯氢管道输送应用验证及科技试验平台，完善材料-零部件-装置-系统多层级试验测试功能。1)采用团队提出的基于载气仓测试装置的氢气输送管道试验系统，实现管路典型部位裂纹和氢气泄漏在线检测，可同时开展至少三类不同规格管道的测试，验证管材抗氢脆焊接技术、高压纯氢管道和关键设备运维安全保障技术;2)应用团队已获得纯氢管道输送工艺，监测平台压力、流动、冲蚀、噪音和振动等信号，验证关键工艺适应性评价方法合理性，完善技术经济合理、安全可靠的纯氢管道输送工艺方案;3)针对管道长度长、监测检测数据量大等特点，建立纯氢管道网络化状态监测与数据智能运维系统，提高平台运行参数控制和数字化管理水平。

任务 2:掺氢管道输送应用验证及科技试验平台

根据实验平台选址、气源、消纳途径及用量，结合材料选型、连接工艺、运维安全、保障等研究成果，借鉴已有掺氢示范平台建设运行经验，建设掺氢管道输送应用验证及科技试验平台。平台上设置管道材料可拆卸试验段，定期进行管道壁厚测定和无损检测，在试验验证完成后，对管道母材和焊缝开展分析测试，评价材料抗氢脆性能指标;平台上设立分支管道，搭建管道材料服役性能评价实验平台，测试温度、压力、流量等参数可控，具备测试管路典型部位裂纹和氢泄漏在线检测(快速定位)功能;在备用管路上预留接口和专用检测(验证)工位，实现设备气密性检测功能和氢气分离等技术验证。

任务 3:面向场景的氢能管道经济性、碳管理研究及氢能管道输送系统构建策略

开展纯氢/掺氢管道输氢技术经济性分析，聚焦典型用氢场景，建立管道输氢成本测算模型，与特高压/高压输电方式进行成本量化对比，对比上游就地制氢再输氢至下游和上游输电至下游再制氢两类方案的技术经济性，从战略层面形成我国重点区域、重点通道中长期输氢规划布局建议;开展纯氢及掺氢管道全生命周期碳管理体系研究，研究管道输氢碳排放核算边界，建立管道输氢全生命周期碳排放核算模型及评价方法，结合上下游场景，研究典型场景下管道输氢碳排放特性，分析管道输氢碳排放影响因素，提出我国氢能管道输送系统发展策略建议。

任务 4:基于深度学习的纯氢及掺氢管道平台数据挖掘技术

融合试验平台运行数据和模拟修正数据，建立基于深度学习的数据挖掘分析技术，形成“平台运行状态-在线监测/检测-数据特征智能识别-算法分析-信息反馈-快速决策“一体化快速安全响应系统。

取得社会经济效益：

(1)科学、技术、产业预期指标

针对我国氢能长输管道管材强度低、输送压力小、输送经验少、规范标准缺的现状，突

破纯氢与天然气掺氢长输管道输送及应用关键技术并开展相关示范验证，预期实现以下目标：形成基于深度学习的纯氢及掺氢管道平台数据挖掘技术，建立面向应用场景的氢能管道输送经济性与全生命周期碳管理分析方法，建设纯氢/掺 氢管道输送应用科技试验平台，申请发明专利 4 项。

(2)科学价值

以“氢相容性-设计制造-适用评价-工艺优化-风险评估-安全保障-应用验证-输氢策略”为主线，攻克纯氢/掺氢天然气管道全尺寸临氢环境服役性能测试评价技术、基于深度学习的纯氢及掺氢管道平台数据挖掘技术、面向应用场景的氢能管道输送经济性与全生命周期碳管理分析技术，具有重要科学价值。

(3)社会、经济和生态效益

通过本课题顺利实施，有利于加快管道输氢应用建设，促进氢能源跨时空调度，带动氢能“制、储、输、用”上中下游全产业链发展，推动氢能终端社会应用，加速实现氢能规模化、产业化、市场化应用。

本人承担主要工作：

指标 5.1:基于深度学习的纯氢及掺氢管道平台数据挖掘技术

管道表面裂纹检测数据等管道安全特征参量通常是典型的时序数据，具有信号复杂多变、数据量大等特点，传统的管道安全检测多基于专家经验和规则系统，如对各种信号特征的定义(基于数学的方法)和抽取、各类阈值的设立，虽此类建模方法对于有规律性的信号可以有效处理，但对于充满噪音、信号复杂多变的场景，系统准确率急剧下降。针对氢能管道的失效模式及安全特征参量，利用深度学习的理论和方法建立管道安全特征参量检测及监测海量数据分析技术，对大量数据进行有效学习并建立自适应的模型，通过对数据逐层变换、逐渐降维至关键编码特征，最后被有效分类预测，提高管道裂纹、氢泄漏监测等数据分析的效率和可靠性。

考核指标				考核方式（方法)及评价手段
指标名称	立项时已有指标值/状态	中期指标值/状态	完成时指标值/状态	
指标 5.1 基于深度学习的纯氢及掺氢管道平台数据挖掘技术: a)有效数据挖掘种类 b)数据识别准确率	深度学习理论框架	a) ≥1 种 b) ≥60%	形成基于深度学习的纯氢及掺氢管道平台数据挖掘技术，并在试验平台应用验证: a)≥2 种 b)≥96%	提交技术报告，通过行业协会/学会组织的同行专家评审，形成评审报告

任务负责人签字（盖章）：

浙江省特种设备科学研究院